



# Phase stability and electronic structures of stoichiometric tantalum mononitrides

Tae-Eun Kim<sup>a</sup>, Seungwu Han<sup>a,\*</sup>, Won-joon Son<sup>b</sup>, Eunae Cho<sup>a</sup>, Hyo-Shin Ahn<sup>a</sup>, Seokmin Shin<sup>b</sup>

<sup>a</sup> Department of Physics, Ewha Woman's University, Seoul 120-750, Republic of Korea

<sup>b</sup> School of Chemistry, Seoul National University, Seoul 151-747, Republic of Korea

## ARTICLE INFO

### Article history:

Received 1 March 2008

Accepted 22 April 2008

Available online 9 June 2008

### PACS:

77.84.Bw

71.20.-b

71.15.Nc

### Keywords:

Tantalum nitrides

Stoichiometric phase

Phase stability

Density functional calculation

Structural property

Electronic structure

Jahn–Teller distortion

## ABSTRACT

Using the density functional methods, we study electronic and structural properties of stoichiometric phases of tantalum mononitride (TaN). The  $\varepsilon$  phase is found to be most stable, closely followed by the  $\theta$  phase. Interestingly, we find that the cubic  $\delta$  phase of the stoichiometric TaN undergoes a spontaneous distortion into a tetragonal structure. This is attributed to a Jahn–Teller type distortion that lifts degeneracy at the Fermi level. The electronic structures indicate that the largest carrier density is expected for  $\delta$ -TaN while  $\theta$ -TaN is close to a quasi-one-dimensional conductor.

© 2008 Elsevier B.V. All rights reserved.

## 1. Introduction

Tantalum mononitride (TaN), a representative refractory nitride, is widely used in many technological applications owing to its outstanding mechanical and chemical stability [1]. For example, TaN is used as hard coating materials or diffusion barriers in micro-electronic devices. The electrical property of TaN can vary between the metal and insulator depending on the  $N_2$  pressure in the growth condition. Recently, additional interest in TaN has been spurred by the high-density electronic devices that employ TaN as a metal gate to be compatible with high-dielectric constant insulators such as  $HfO_2$  [2]. Thermal stability of TaN prevents the performance degradation after post-deposition annealing.

TaN is also known for its variety in compositions and metastable phases. The substoichiometric  $\delta$ - $TaN_x$  with cubic symmetry has been studied most extensively to date. This cubic phase can support a large density of vacancies up to 20%. On the other hand, three stable phases have been known for TaN close to the 1:1 stoichiometry. At ambient conditions, the hexagonal  $\varepsilon$  phase with the space group of  $P6_3m$  is known to be stable [3]. This structure is close to the more symmetric CoSn ( $P6/mmm$ ) type. (Some litera-

ture indicates the CoSn structure as the  $\varepsilon$  phase [1,4].) The  $\varepsilon$  phase transforms to the hexagonal  $\theta$  phase (space group of  $P6m2$ , WC-type) at high pressure conditions [5], or to the cubic  $\delta$  phase (space group of  $Fm\bar{3}m$ ) with the rocksalt structure at high temperatures [6]. These structures are displayed in Fig. 1(a)–(c). Compared to the cubic  $\delta$  phase [4,7–10],  $\varepsilon$  and  $\theta$  phases have not been studied much and there is no first-principles calculation on their electronic structures as far as we are aware. (A theoretical analysis based on empirical methods is available for the  $\theta$  phase [5].) Motivated by this lack of basic information, we perform in this work first-principles calculation on stoichiometric phases of TaN. The atomic and electronic structures are compared and analyzed in detail.

## 2. Computational methods

All numerical results including total energies, density of states (DOS), and band structures are obtained by the density functional methods. We use a computational code of Vienna *ab initio* simulation package (VASP) [11]. The generalized gradient approximation with a functional form suggested in Ref. [12] is used to describe the exchange and correlation energies of electrons. For Ta atoms, we use a pseudopotential that considers semicore levels as frozen, i.e.,  $5d^36s^2$  as valence configurations. The energy cut-off for the plane-wave expansion is set to 500 eV. The energy levels are

\* Corresponding author. Tel.: +82 2 3277 4067; fax: +82 2 3277 2372.  
E-mail address: [hansw@ewha.ac.kr](mailto:hansw@ewha.ac.kr) (Seungwu Han).

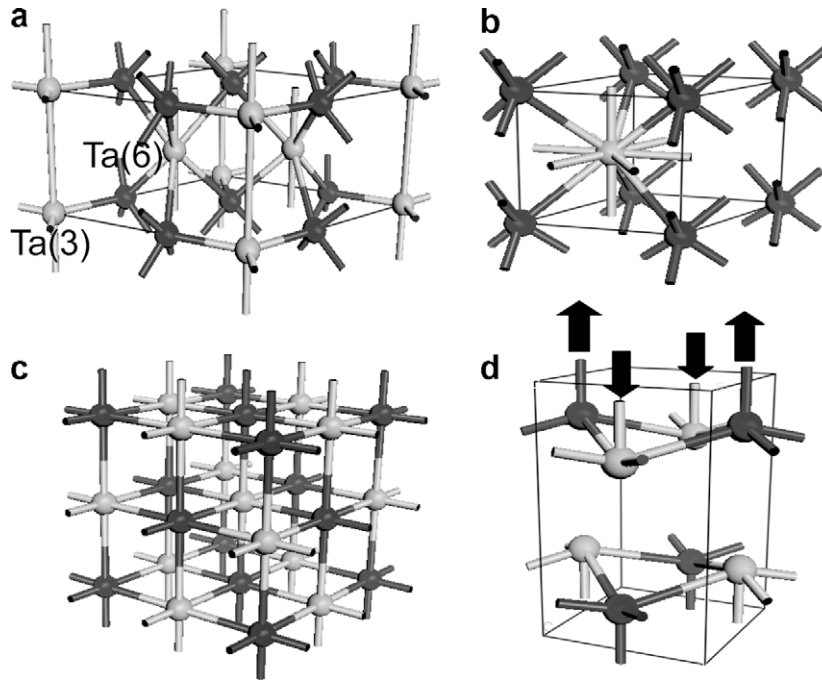


**Fig. 1.** Unit cells of various phases of tantalum mononitride (TaN). Ta and N atoms are shown as pale and dark balls, respectively. (a)  $\varepsilon$  Phase, (b)  $\theta$  phase, (c)  $\delta$  phase (conventional cell), and (d) tetragonal structure ( $\delta'$ -TaN, see text for explanation). The arrows in (d) show a corrugation pattern by which the  $\delta$  phase is distorted into the tetragonal symmetry.

broadened based on the second-order Methfessel–Paxton scheme [13] with a width of 0.2 eV. For the  $k$ -point integration within the first Brillouin zone, regular meshes of  $6 \times 6 \times 10$ ,  $8 \times 8 \times 8$ ,  $8 \times 8 \times 8$  and  $7 \times 7 \times 4$  are used for primitive cells of  $\varepsilon$ ,  $\theta$ ,  $\delta$ , and  $\delta'$  phases, respectively. (See below for the explanation of  $\delta'$ -TaN.) By increasing the energy cut-off and  $k$ -point density for the  $\delta$  phase up to 900 eV and  $14 \times 14 \times 14$ , respectively, it was confirmed that the selected computational parameters attain the convergence of the total energy ( $<10$  meV/atom), Hellmann–Feynman forces on each atom ( $<0.02$  eV/Å), and stress tensors ( $<5$  kbar) to desired levels.

### 3. Results and discussion

#### 3.1. Equilibrium structures

To obtain equilibrium lattice parameters for the three stoichiometric phases of TaN, the ionic configurations and lattice vectors were fully optimized. The equilibrium lattice parameters for each structure are compiled in Table 1. The computed values agree with experimental data within 0.7%. Compared to other phases,  $\delta$ -TaN shows the largest discrepancy with the experiment and this is likely to be caused by high defect densities inherent for the  $\delta$  phase. The lattice parameter of  $\delta$ -TaN is calculated to be 4.41 Å which compares favorably with the all-electron result of 4.42 Å [7]. Interestingly, we find that the cubic structure with the strictly 1:1 composition is unstable; when the symmetry is lowered by a slight deformation, the structure spontaneously changes to a tetragonal shape with columns along the  $c$ -axis buckling alternatively. This phase is tentatively named as  $\delta'$ -TaN. The equilibrium lattice parameters of  $\delta'$ -TaN in Table 1 indicate that the  $ab$ -plane is compressed by 5% while the  $c$ -axis is elongated by as much as 15.5%. Fig. 1(d) shows the final structure obtained in this way, with the arrows representing the buckling pattern. The observed instability of the cubic phase is in line with unstable phonon modes [14] or negative defect formation energies [8]. The symmetry lowering

from the cubic to tetragonal shape is related to a Jahn–Teller distortion that lifts degeneracy at the Fermi level, as will be discussed in the below section.

#### 3.2. Relative stability and bonding properties

We compare the stability between different phases by calculating the heat of formation ( $\Delta H_f$ ) as defined in the following:

$$\Delta H_f = E_{\text{tot}}(\text{bcc-Ta})/n_{\text{Ta}} + E_{\text{tot}}(\text{N}_2)/2 - E_{\text{tot}}(\text{TaN})/n_{\text{N}}, \quad (1)$$

where  $E_{\text{tot}}$  is the total energy of the system in the parenthesis and  $n_{\text{N}}$  ( $n_{\text{Ta}}$ ) is the number of nitrogen (tantalum) atoms within the unit cell. The computational results are shown in Table 1. It can be seen from the table that the stability at zero temperature is in the sequence of  $\varepsilon > \theta > \delta' > \delta$ , which is consistent with the fact that  $\varepsilon$ -TaN is the equilibrium phase at ambient conditions. We also consider the symmetric CoSn structure for comparison purpose. The

**Table 1**

Space group, heat of formation ( $\Delta H_f$ ), lattice parameters, distances between nearest-neighbored atoms of four crystal structures of TaN studied in this work

Phase	Space group	$\Delta H_f$ (eV/f.u.)	Lattice parameters (theory, Å)	Lattice parameters (experiment, Å)	$d_{\text{Ta-Ta}}$ (Å)	$d_{\text{Ta-N}}$ (Å)
$\varepsilon$	$P\bar{6}2m$	2.39	$a = 5.226$	$a = 5.196^a$	2.920	2.054
			$c = 2.920$	$c = 2.911$	3.017	2.173
$\theta$	$P\bar{6}m2$	2.36	$a = 2.946$	$a = 2.936^b$	2.897	2.234
			$c = 2.897$	$c = 2.885$	2.946	
$\delta$	$Fm\bar{3}m$	1.75	$a = 4.414$	$a = 4.385^c$	3.121	2.207
$\delta'$	$P4/$	1.92	$a = 2.966$	–	2.966	2.167
	$nmm$		$c = 5.099$		3.124	2.238

For comparison purposes, experimental data are also shown.

<sup>a</sup> Ref. [3].

<sup>b</sup> Ref. [15].

<sup>c</sup> Ref. [16].

calculated  $\Delta H_f$  is 1.49 eV, smallest among the structures studied in this work.

The bond lengths of Ta–Ta and Ta–N pairs ( $d_{\text{Ta–Ta}}$  and  $d_{\text{Ta–N}}$ , respectively) are also shown in Table 1. The nearest-neighbor distance between Ta atoms in the crystalline bcc structure is calculated to be 2.865 Å based on the same computational setup. There are two types of Ta atoms in  $\varepsilon$ -TaN and they are denoted as Ta(3) and Ta(6), with the numbers in parentheses indicating the coordination number of neighboring nitrogen atoms. (See Fig. 1(a).) In  $\varepsilon$ -TaN, the shortest  $d_{\text{Ta–Ta}}$  (2.920 Å) is found for Ta(3)–Ta(3) and Ta(6)–Ta(6) pairs along the  $c$ -axis. The next closest pair is Ta(6)–Ta(6) along the middle plane with a separation of 3.027 Å. On the other hand, the shortest Ta–Ta distances are 2.897 and 2.946 Å in  $\theta$ -TaN. These values are substantially smaller than those in other phases and very close to that of the bulk bcc-Ta crystal. This implies that the metallic bonding character is most enhanced in  $\theta$ -TaN among the four phases. In contrast, the shortest  $d_{\text{Ta–N}}$  is found for  $\varepsilon$ -TaN, suggesting that the covalent or ionic character is dominant in this phase. The small difference in  $\Delta H_f$  be-

tween these two phases (0.03 eV/f.u.) suggests that the stability is in a delicate balance between the two competing bonding natures. On the other hand,  $d_{\text{Ta–Ta}}$  is largest in  $\delta$ -TaN among the four phases, which accounts for the smallest  $\Delta H_f$ . The deformation to the tetragonal  $\delta'$ -TaN reduces  $d_{\text{Ta–Ta}}$  by as much as 0.155 Å in a plane normal to the  $c$ -axis ( $ab$ -plane). By contrast,  $d_{\text{Ta–N}}$  changes by only  $\sim 0.04$  Å. Therefore, the rearrangements in the bonding distribution lead to the enhanced Ta–Ta bonding in the  $ab$ -plane, which significantly affects electronic structures as will be discussed in the below section. This would be a main driving force to distort the symmetric structure of  $\delta$ -TaN.

### 3.3. Electronic structures

Next we compare the electronic structure of each phase. The computed DOS is shown in Fig. 2. The decomposition of the bands indicates that the low lying states around  $-17$  eV are mixed characters of Ta-s and N-s orbitals, resulting in the  $ss\sigma$  bonding. The valence bands between  $-10$  and  $-3$  eV consist of Ta-d and N-p orbitals (see Fig. 3), and therefore the bonding type is  $dp\sigma$  or  $dp\pi$ . The electronic states around the Fermi level are dominated by Ta-d characters. This means that the metallic bonding character prevails at these energy ranges. A dip at the Fermi level is noticeable in DOS of all phases except for  $\delta$ -TaN. In particular, DOS of the  $\theta$  phase shows a structure close to the semimetallic one. In contrast, DOS at the Fermi level is substantially large for  $\delta$ -TaN, implying the highest electronic conductivity. This is well correlated with its application as electronic conductors.

The band structures of the four phases are shown in Fig. 3. The band structure of  $\delta$ -TaN in Fig. 3(c) is very similar to the full-potential result in Ref. [7], assuring the accuracy of the method employed in this work. For the  $\theta$  phase, there are few bands crossing the Fermi level, and this is consistent with the smallest DOS at this energy (see Fig. 2(b)). In addition, a large dispersion is noticeable along the  $\Gamma$ –A direction, which is due to the shortest length between Ta atoms along the  $c$ -axis (see Table 1). This means that  $\theta$ -TaN behaves like one-dimensional conductor with a highly anisotropic Fermi surface between  $ab$ - and  $c$ -directions. On the other hand, it is notable that the Fermi level of  $\delta$ -TaN closely passes a degeneracy point near the  $W$ -point. This degeneracy is found to be lifted in the band structure of  $\delta'$ -TaN with a gap opening of 1.6 eV. (See an arrow in Fig. 3(d); the  $A$ -point in the tetragonal cell of  $\delta'$ -TaN corresponds to the  $W$ -point in the face-centered-cubic structure of  $\delta$ -TaN.) This strongly supports that the degeneracy at the Fermi level is the origin of structural instability and the distortion is a Jahn–Teller type.

## 4. Conclusion

In summary, we have calculated on the various phases of TaN with the stoichiometric composition. The stability is in the order of  $\varepsilon > \theta > \delta' > \delta$ . It was found that the cubic  $\delta$ -TaN undergoes a spontaneous distortion into a tetragonal structure caused by the Jahn–Teller type distortion that lifts degeneracy at the Fermi level. The electronic structures were closely examined and it was found that the largest carrier density is expected for  $\delta$ -TaN while  $\theta$ -TaN is close to a quasi-one-dimensional conductor.

## Acknowledgements

This work was supported by the System IC2010 program. The computations were carried out at Korea Institute of Science and Technology Information (KSC-2007-S00-1006).

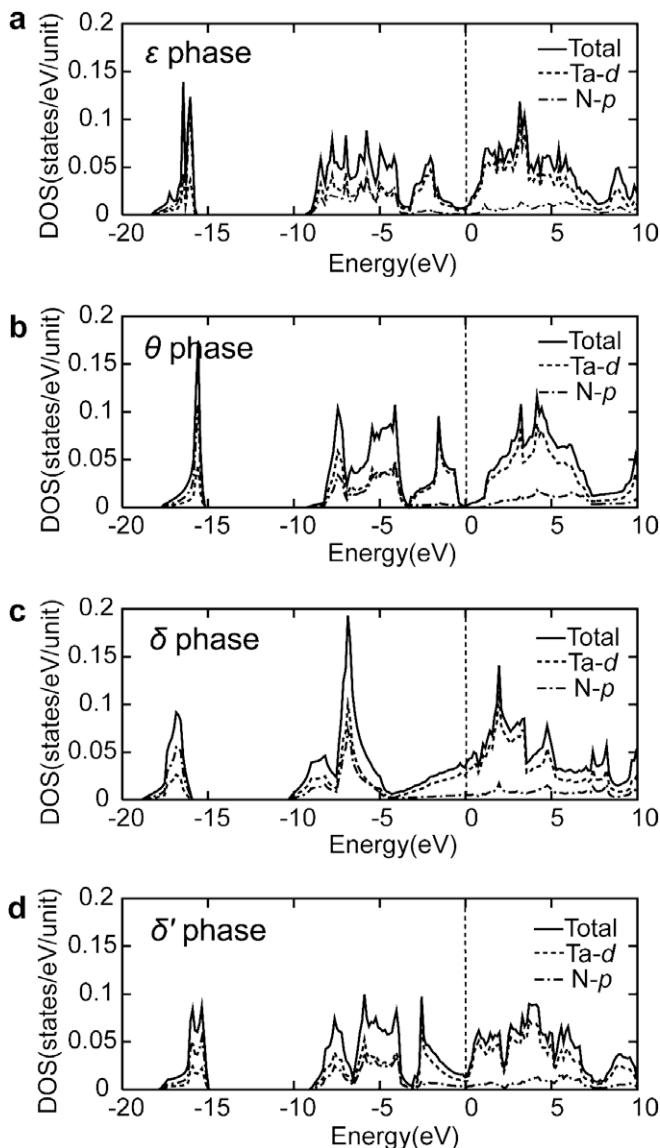


Fig. 2. Total and partial density of states (DOS) for stoichiometric phases of TaN. DOS is normalized by formula unit.

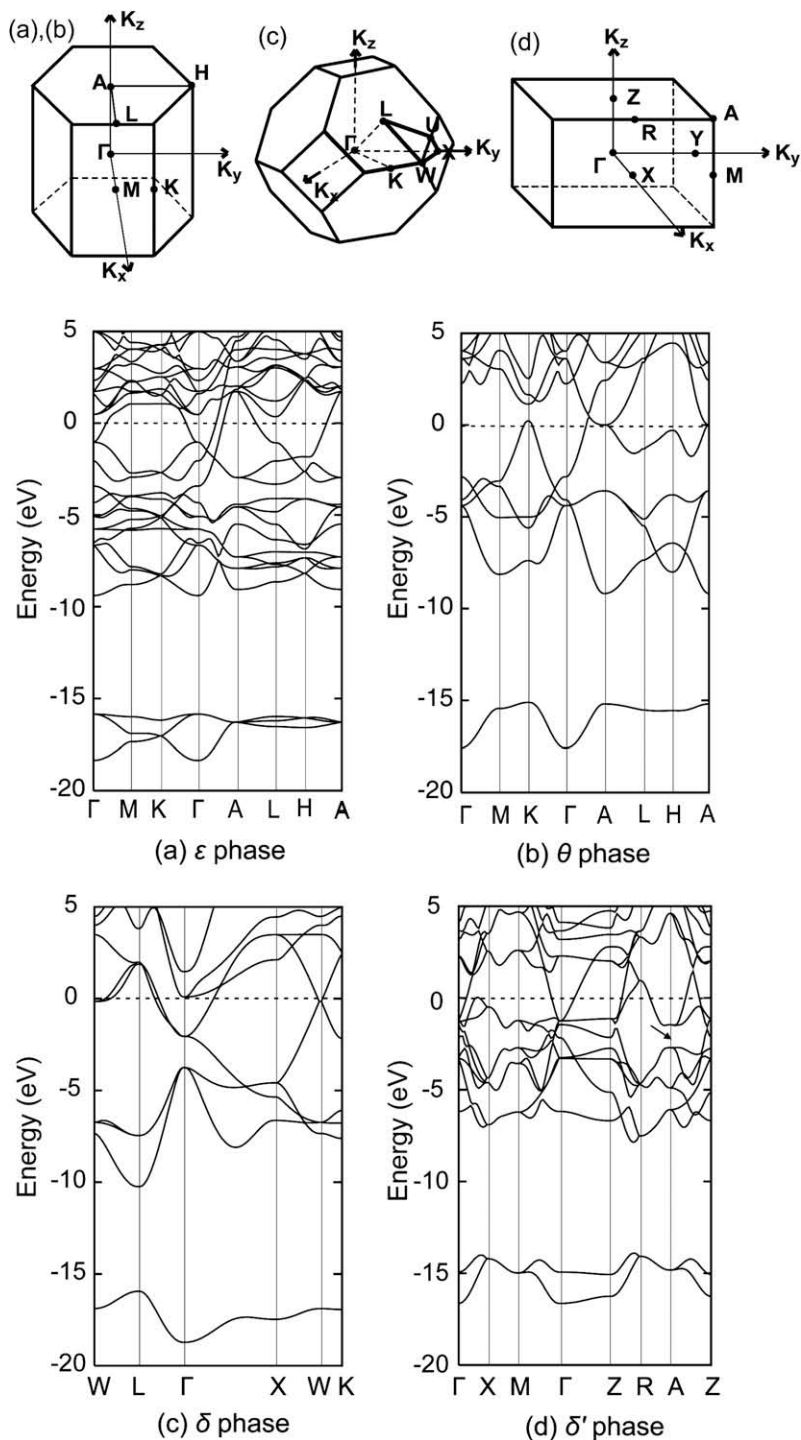


Fig. 3. The band structure of various phases of TaN. The first Brillouin zone is shown on the top.

## References

- [1] L.E. Toth, Transition Metal Carbides and Nitrides, Academic Press, New York and London, 1971.
- [2] C.S. Kang, H.-J. Cho, Y.H. Kim, R. Choi, K. Onishi, A. Shariar, J.C. Lee, J. Vac. Sci. Technol. B 21 (2003) 2026.
- [3] A.N. Christensen, B. Lebeck, Acta Crystallogr. B 34 (1978) 261.
- [4] C. Stampfl, A.J. Freeman, Phys. Rev. B 71 (2005) 024111.
- [5] A.V. Tsvyashchenko, S.V. Popova, E.S. Alekseev, Phys. Status Solidi (b) 99 (1980) 99.
- [6] J. Gatterer, G. Dufek, P. Ettmayer, R. Kieffer, Monatsh. Chem. 106 (1975) 1137.
- [7] M. Sahnoun, C. Daul, M. Driz, J.C. Parlebas, C. Demangeat, Comp. Mater. Sci. 33 (2005) 175.
- [8] L. Yu, C. Stampfl, D. Marshall, T. Eshrich, V. Narayanan, J.M. Rowell, N. Newman, A.J. Freeman, Phys. Rev. B 65 (2002) 245110.
- [9] C. Stampfl, A.J. Freeman, Phys. Rev. B 67 (2003) 064108.
- [10] J. Häglund, A. Fernández Guillermet, G. Grimvall, M. Körling, Phys. Rev. B 48 (1993) 11685.
- [11] G. Kresse, J. Hafner, Phys. Rev. B 47 (1993) R558 ; 49 (1994) 14251.
- [12] J.P. Perdew, K. Burke, M. Ernzerhof, Phys. Rev. Lett. 77 (1996) 3865.
- [13] M. Methfessel, A.T. Paxton, Phys. Rev. B 40 (1989) 3616.
- [14] E.I. Isaev, S.I. Simak, I.A. Abrikosov, R. Ahuja, Yu. Kh.Yu.Kh. Vekilov, M.I. Katsnelson, A.I. Lichtenstein, B. Johansson, J. Appl. Phys. 101 (2007) 123519.
- [15] G. Brauer, A. Skokan, A. Neuhaus, E. Mohr, Monatsh. Chem. 103 (1972) 794.
- [16] W.B. Pearson (Ed.), Structure Reports, Vol. 35A, International Union of Crystallography, Oosthoek, Scheltema, and Holkema, Utrecht, 1913, p. 121.